

Cassini thermal observations of Saturn's main rings: Implications for particle rotation and vertical mixing

Linda J. Spilker^{a,*}, Stuart H. Pilorz^a, Brad D. Wallis^a, John C. Pearl^b, Jeffrey N. Cuzzi^c,
Shawn M. Brooks^a, Nicolas Altobelli^a, Scott G. Edgington^a, Mark Showalter^d,
F. Michael Flasar^b, Cecile Ferrari^e, Cedric Leyrat^e

^a*Jet Propulsion Laboratory/California Institute of Technology, Pasadena, CA, USA*

^b*Goddard Spaceflight Center*

^c*NASA Ames Research Center*

^d*SETI Institute*

^e*AIM, CEA Saclay & University Paris 7*

Accepted 4 May 2006

Available online 26 July 2006

Abstract

In late 2004 and 2005 the Cassini composite infrared spectrometer (CIRS) obtained spatially resolved thermal infrared radial scans of Saturn's main rings (A, B and C, and Cassini Division) that show ring temperatures decreasing with increasing solar phase angle, α , on both the lit and unlit faces of the ring plane. These temperature differences suggest that Saturn's main rings include a population of ring particles that spin slowly, with a spin period greater than 3.6 h, given their low thermal inertia. The A ring shows the smallest temperature variation with α , and this variation decreases with distance from the planet. This suggests an increasing number of smaller, and/or more rapidly rotating ring particles with more uniform temperatures, resulting perhaps from stirring by the density waves in the outer A ring and/or self-gravity wakes.

The temperatures of the A and B rings are correlated with their optical depth, τ , when viewed from the lit face, and anti-correlated when viewed from the unlit face. On the unlit face of the B ring, not only do the lowest temperatures correlate with the largest τ , these temperatures are also the same at both low and high α , suggesting that little sunlight is penetrating these regions.

The temperature differential from the lit to the unlit side of the rings is a strong, nearly linear, function of optical depth. This is consistent with the expectation that little sunlight penetrates to the dark side of the densest rings, but also suggests that little vertical mixing of ring particles is taking place in the A and B rings.

© 2006 Elsevier Ltd. All rights reserved.

Keywords: Saturn's rings; Cassini; Cassini composite infrared spectrometer; Thermal ring measurements

1. Introduction

The factors that determine the temperature distribution across the surface of an individual ring particle are more complex and more time-variable than those for an isolated body, such as an asteroid. When they pass through Saturn's shadow, ring particles are cut off from incoming solar insolation, which generally provides the dominant thermal forcing. Radiating at 95 K, Saturn is also a

significant source of thermal radiation for the rings, and although Saturn's thermal input is constant for a ring particle on a circular orbit, it drops by roughly a factor of four from the innermost C ring to the outermost A ring. Light reflected from Saturn's sunlit hemisphere provides a third heat source that strongly varies as a function of the particle's position in its orbit (hour angle). Also, when the ring is dense enough, nearby particles can be a significant heating source for one another. Therefore, the thermal input across the surface of a ring particle varies substantially as it circles the planet. For instance, a particle at midnight (a local hour angle of 0°) is heated only by

*Corresponding author. Tel.: +1 818 354 1647; fax: +1 818 393 4495.

E-mail address: Linda.J.Spilker@jpl.nasa.gov (L.J. Spilker).

Saturn's thermal emission and only on its subsolar hemisphere, while its nightside radiates to space or neighboring particles. At local noon (local hour angle of 180°), it is heated by all three sources: the Sun heats its dayside and Saturn heats its nightside by both thermal emission and reflected sunlight (Ferrari and Leyrat, 2006).

The response of an individual ring particle to these radiative inputs is dictated further by the particle's albedo, rotation and the thermal inertia, Γ , of its surface. In general, the sunlit hemisphere of a particle is expected to be warmer than the dark, unlit hemisphere. The observed fraction of a particle lit by the Sun is described by the phase angle, α , i.e., the Sun-particle-observer angle. Just as in the case of an isolated asteroid, the spin of a ring particle carries the warmest part of its surface away from the location of maximum thermal forcing, by an amount determined by the thermal inertia of the particle's surface (Spencer et al., 1989).

Whether this thermal forcing manifests itself as a discernible temperature gradient across the surface of a ring particle depends on the particle's thermal inertia and rotation rate. In most cases, if the particle's Γ is high (in other words, it is resistant to temperature change), and/or if it rotates rapidly, surface temperature variations will be muted. If Γ is low, temperature gradients on the surface due to changing input flux will be enhanced. The observed variations in particle temperature along the orbit are then characteristic of how rapidly the particle rotates and how fast it re-radiates its thermal energy.

Numerical simulations of the collisional dynamics of Saturn's rings show that meter-sized particles, representing the bulk of the ring mass, concentrated along the ring plane. The smaller particles are scattered into a thicker halo (Salo, 1987; Richardson, 1994; Salo and Karjalainen, 2003; Ohtsuki and Toyama, 2005). Ring particles probably have rough, irregular surfaces (Cuzzi et al., 2002; Poulet et al., 2002), so that oblique impacts between particles lead to particle rotation and the vertical dispersion of the smaller particles. When a single particle size is considered, simulations suggest that the particles rotate slowly (Araki, 1991; Salo 1995). When a more realistic power law distribution is used, simulations show that the smaller particles tend to spin faster and are more vertically dispersed than the large ones (Richardson, 1994). Small particles have a random spin orientation while large particles have spin axes that are aligned nearly normal to the ring plane (Ohtsuki and Toyama, 2005). Dynamical models predict rotation rates that range from 10Ω for smaller particles to 0.1Ω for larger particles (Ohtsuki, 2005), where Ω is the orbital mean motion (rad/s).

Ring particles orbit within a swarm of other particles, adding further complexity. Particles orbit in Keplerian motion around Saturn. Collisions perturb this motion occasionally in a thin ring and more systematically in denser rings. Vertical excursions about the ring plane are expected although these excursions can be limited by mutual attraction between particles if closely packed

(Salo, 1995). In this case, large particles may form several layers with gaps filled with smaller particles (Richardson, 1994). The vertical dynamics of particles in such rings have not been explored numerically. Without vertical obstruction, a particle is expected to spend half of its orbit on the lit face and half on the unlit face of the ring, in the shadow of lit particles. In a monolayer, particles are in the mid-plane and do not suffer this semi-diurnal eclipse. Thermal gradients between lit and unlit faces of a multilayer ring are expected. They may be also present in a monolayer ring if the surface temperature of particles is not uniform. The thermal gradient is expected to vary seasonally, as the amount of sunlight filtering through the rings depends upon the solar elevation angle, B' , above the ring plane. It may also depend on the ring density as mutual shadowing or sunlight absorption increases with ring optical depth, τ . The temperature measured by CIRS may also depend on Cassini's elevation angle, B , the angle between the ring plane and a line to the spacecraft.

Consequently, the observed thermal emission of the rings is expected to depend on particle albedo, spin rate, spin orientation, α , B' , B , local hour angle, radial location within the rings, and τ . Observations at a variety of viewing geometries are necessary to retrieve the properties of the rings' constituent particles such as Bond albedo, thermal inertia, rotation rate, and their local vertical dynamics. Ground-based observations are relatively restricted because the viewing angles are limited to $\alpha \leq 6^\circ$. The Cassini mission, with 74 orbits at various orientations and inclinations, provides an ideal opportunity to increase our understanding of particle properties and local dynamics using CIRS measurements.

In this paper, we derive ring temperatures from thermal infrared radial scans across the A, B and C rings, and the Cassini Division at low and high α for both the lit and unlit faces of the rings. A summary of pre-Cassini thermal infrared observations is presented in Section 2. In Section 3, we describe our observations and our analysis methods. Results presented in Section 4 are discussed in Section 5. Conclusions are presented in Section 6 and future observations are outlined in Section 7.

2. Pre-Cassini thermal infrared ring observations

Observers have measured the thermal radiation from Saturn's ring particles at wavelengths from roughly $10\ \mu\text{m}$ to $1\ \text{cm}$ (wavenumbers of 1000 to $1\ \text{cm}^{-1}$). Discussions of previous spacecraft and ground-based thermal measurements are given by Cuzzi et al. (1984), Esposito et al. (1984) and Spilker et al. (2003). Pioneer 11 infrared radiometer observations at 20 and $45\ \mu\text{m}$, with $B' = -2^\circ$ (south of the ring plane), were the first to spatially resolve the rings (Froidevaux and Ingersoll, 1980). The Voyager infrared spectrometer (IRIS) obtained thermal observations of Saturn's rings in 1980 and 1981 from 200 to $650\ \text{cm}^{-1}$ (50 – $17\ \mu\text{m}$) with $B' = 4^\circ$ and 8° (north of the ring plane) (Hanel et al., 1981, 1982). Additional ground-based

measurements of ring thermal emission are reported by Roellig et al. (1988), Spilker et al. (2003) and Ferrari et al. (2005).

The rings have also been observed as the particles are eclipsed by Saturn's shadow. The abrupt change in solar illumination suffered by particles while crossing the planetary shadow produces thermal transients that help determine the thermal inertia of the particles. The thermal inertia, Γ , of a homogeneous particle is related to the volumetric thermal properties of the material by $\Gamma = (\kappa\rho C_p)^{1/2}$ ($\text{J m}^{-2} \text{K}^{-1} \text{s}^{-1/2}$), where κ is thermal conductivity ($\text{J K}^{-1} \text{m}^{-1} \text{s}^{-1}$), ρ the density (kg m^{-3}) and C_p the heat capacity at constant pressure ($\text{J K}^{-1} \text{kg}^{-1}$). For a nonporous particle of normal ice Ih at a typical ring temperature of 80 K, $\kappa_{\text{ice}} = 8.1 \text{ J K}^{-1} \text{m}^{-1} \text{s}^{-1}$ (Slack, 1980), $\rho_{\text{ice}} = 918 \text{ kg m}^{-3}$ and $C_{p_{\text{ice}}} = 720 \text{ J K}^{-1} \text{kg}^{-1}$ (Schulman, 2004), so that $\Gamma_{\text{ice}} = 2310 \text{ J K}^{-1} \text{m}^{-2} \text{s}^{-1/2}$. This, however, is an upper limit because porosity substantially reduces both the density and the thermal conductivity. The first dedicated spacecraft observations at $20 \mu\text{m}$, (Froidevaux et al., 1981) favored low Γ particle surfaces similar to water frost on the Galilean satellite surfaces because of observed rapid heating of the particles after exit from eclipse, about 6 K in 1.7 h in the B ring. More recent measurements show that $\Gamma \sim 5 \text{ J m}^{-2} \text{K}^{-1} \text{s}^{-1/2}$, for a temperature increase of 4 K in 2.7 h in the same ring if the particles are confined to a monolayer (Ferrari et al., 2005). Quantitative estimation of the thermal inertia from the Froidevaux measurements suggest higher values, $\Gamma \sim 16 \pm 13 \text{ J m}^{-2} \text{K}^{-1} \text{s}^{-1/2}$. Such low thermal inertia is characteristic of a frosty regolith and very porous particle aggregates (Ferrari et al., 2005). For comparison, the high albedo regions of Europa, and of the other Galilean satellites and the Saturnian satellites like Rhea, Dione and Tethys, have $\Gamma = 30\text{--}70 \text{ J m}^{-2} \text{K}^{-1} \text{s}^{-1/2}$ (Spencer et al., 1989, 1992). Recent CIRS measurements of Enceladus provide $\Gamma = 15\text{--}30 \text{ J m}^{-2} \text{K}^{-1} \text{s}^{-1/2}$ (Spencer et al., 2006). The thermal inertias of Chiron and Asbolus centaurs are estimated at $\Gamma \leq 10 \text{ J m}^{-2} \text{K}^{-1} \text{s}^{-1/2}$ (Fernandez et al., 2002; Groussin et al., 2000).

Voyager infrared observations provided information about the ring particle rotation states. IRIS observed the C ring particles at both low and high α as they passed into Saturn's shadow (Hanel et al., 1981). A larger drop in temperature was observed at low α than at high α , indicating that the night hemispheres of the particles are colder than the day hemispheres. This behavior suggests slowly rotating particles. A similar contrast in temperature was found in a reanalysis of the Voyager data on the C ring (Spilker et al., 2006a). Measurements at low α also preclude fast rotators for both the B and C rings because the observed temperatures are too high to be fit by the models (Ferrari et al., 2005).

The temperature differences between lit and unlit faces of A and B rings were first estimated using Pioneer radiometer data by Froidevaux and Ingersoll (1980) giving $\Delta T = T_{\text{LIT}} - T_{\text{UNLIT}} \sim 17$ and 14 K, respectively when the

Sun was 2° south of the ring plane. The Voyager IRIS spectra were analyzed assuming an isothermal semitransparent nonscattering slab, with emissivity $(1 - e^{-\tau/\sin B})$ (Hanel et al., 1981, 1982). On the illuminated face, the A and B ring temperatures were nearly the same, 69 ± 1 and 68 ± 1 K, respectively; the C ring and Cassini Division were warmer, 85 ± 1 and 85 ± 2 K, respectively. Reasons for the higher temperatures include lower visual albedos (Smith et al., 1981), much lower τ , and relatively little interparticle shadowing within the C ring and Cassini Division.

3. CIRS ring observations and data analysis

3.1. Observations

The CIRS instrument on Cassini consists of two Fourier transform spectrometers, which together measure thermal emission from 1400 to 10 cm^{-1} ($7 \mu\text{m}$ to 1 mm) at an apodized spectral resolution programmable from 0.5 to 15.5 cm^{-1} (Kunde et al., 1996; Flasar et al., 2004). The far infrared interferometer covers from 600 to 10 cm^{-1} ($17 \mu\text{m}$ to 1 mm) and has a circular field of view that is 4 mrad in diameter. The mid-infrared interferometer consists of two 1×10 arrays of 0.3-mrad pixels, which together span $1400\text{--}600 \text{ cm}^{-1}$ ($7\text{--}17 \mu\text{m}$). For the observations of the main rings reported here, we used data from the single far infrared detector (Focal Plane 1 or FP1).

After Cassini's insertion into Saturn orbit in mid-2004, the CIRS instrument began acquiring spatially resolved scans of Saturn's main rings (Flasar et al., 2005). Thermal spectra of the rings have been obtained at a number of α , ring local times and B .

For this paper we discuss four radial scans that were obtained at different ring geometries; two on the lit face of the rings, at low ($\alpha \sim 30^\circ$) and high phase ($\alpha \sim 135^\circ$), and two on the unlit face of the rings, again at low ($\alpha \sim 50^\circ$) and high phase ($\alpha \sim 135^\circ$) (Spilker et al., 2005). The lit scans were taken on the afternoon ansa, where the temperatures are likely to have stabilized. The unlit scans were taken on the morning ansa where a small amount of warming may still be taking place. The circular CIRS FP1 instrument field of view slowly scanned radially across the rings at a radial resolution of $2000\text{--}2600 \text{ km}$ per footprint (see Fig. 1). The Sun illuminated the south face of the rings with B' between -22° and -23° ; the spacecraft elevation, B , was between 6.6° and -7.3° . Deep space spectra off the rings were also

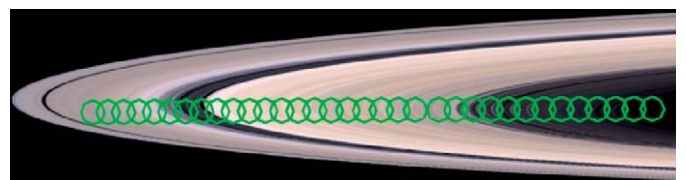


Fig. 1. The lit high- α radial scan is shown. The green CIRS FP1 footprints are displayed for every 35th footprint.

taken for calibration purposes. The observation parameters are summarized in Table 1.

3.2. Data analysis

We define a ring particle temperature by assuming that each FP1 spectrum, I_ν , is a scaled blackbody function:

$$I_\nu = \beta_\nu B_\nu(T_{\text{eff}}), \quad (1)$$

where ν is the wavenumber, β_ν the scale factor and $B_\nu(T_{\text{eff}})$ the Planck function for material at a temperature, T_{eff} . A single Planck function provides an excellent fit to our spectra to within errors, as is expected if the emitting surfaces have a nearly uniform temperature distribution; under such circumstances, the single temperature that is fit will be close to the weighted mean temperature of such an ensemble of emitters. T_{eff} in the above formula will be greater than the minimum temperature of the emitting surfaces in FP1 and less than the maximum temperature, and will be weighted by the projected surface area emitting at any temperature. The factor β_ν includes the effects of filling factor, ring τ , particle emissivity, interparticle shadowing, and geometrical effects related to the observation angle. We restrict our analyses to the spectral region between 100 and 400 cm^{-1} (100–25 μm) because it contains the peak of the Planck function for the range of expected ring temperatures, the signal-to-noise ratio is high and because the resulting β_ν is essentially independent of wavenumber in this interval (Spilker et al., 2006).

For each spectrum, we derive β and T_{eff} simultaneously as the values that minimize the weighted residuals between the spectrum and a theoretical spectrum defined by Eq. (1):

$$R(T, \beta) = \sum_\nu [(I_\nu - \beta_\nu B_\nu(T_{\text{eff}}))/\sigma_\nu]^2. \quad (2)$$

Here σ is the instrument noise equivalent spectral radiance (NESR—see Flasar et al., 2004). We expect that the quantity, R , is approximately χ^2 distributed with $N-2$ degrees of freedom (as there are N independent wavenumbers in the spectrum). We have verified this result by looking at the variation of R over long scans involving

multiple spectra of the same target. To evaluate the error bounds, we utilize the theorem that perturbations to R resulting from varying T and β will also be χ^2 distributed, with two degrees of freedom (Press et al., 1992). We evaluate the region around the best fit spectrum in the T – β plane, within which the value of R falls within the 68.2% tail of the χ^2 distribution, i.e., where $R(T', \beta') - R(T, \beta) < 2.31$, and take the bounds in temperature and β as the extreme values within that region.

Sample fits to spectra from the lit B ring are shown in Fig. 2, along with contours derived by subtracting the χ^2 value of the best fit (the minimum value) from the χ^2 value derived from applying Eq. (2) at each point in the T – β plane. Overlain in red is the contour, derived from a Taylor series approximation to the theoretical $\Delta\chi^2$ values in the region of the best fit, within which 68% of random perturbations to the best fit spectrum (using noise equivalent to the NESR at each wavenumber) would be expected to lie. In all cases, the deviations of our simple, single-temperature fit from the observed spectrum are less than the NESR, i.e., all of the values ‘ R ’ that we calculate are within the range expected from noise at the level of the NESR. The NESR is overlain as a dashed line.

The heavy contour in the lower panels represents one within which perturbations of the spectrum would be expected to lie, and the points within it are the results of 1000 realizations of adding random noise to the best fit, with a standard deviation equal to the instrument NESR. Further details of our fitting process and the behavior of T_{eff} and β_ν with wavenumber are described by Spilker et al. (2006).

4. Results

We examine two aspects of the radial dependence of temperature within the main rings. First, we compare the phase angle dependence for both the lit and unlit faces of the rings. Then, we explore the correlation between temperature variations and ring optical depth.

Table 1
Geometry data for radial ring scans

Observation type	Start time	Duration (h:min)	B' , solar elevation angle (deg.)	Range (R_s)	B , Cassini elevation angle (deg.)	α , phase angle (deg.)	Hour angle (deg.)
Lit low α (red curve)	2005-104T06:54	02:57	–22.01	9.143 10.667	–7.09 –7.32	26.83 35.81	239.90 240.0
Lit high α (gold curve)	2004-350T21:36	01:32	–23.13	9.817 10.499	–6.13 –6.47	130.49 137.38	311.56 315.95
Unlit low α (blue curve)	2004-349T19:57	01:32	–23.14	7.453 7.439	6.59 6.45	47.50 60.40	122.72 129.74
Unlit high α (green curve)	2005-105T11:56	01:28	–22.00	9.362 9.773	3.53 3.31	131.50 140.49	142.2 142.32

B' is negative because the Sun is on the south face of the rings. R_s is 60,330 km. B is measured from the equator and is negative on the south (lit) face of rings and positive on the north (unlit) face of the rings. Hour angle is defined as 0° at local midnight, 90° at 6 a.m., 180° at noon, and 270° at 6 p.m.

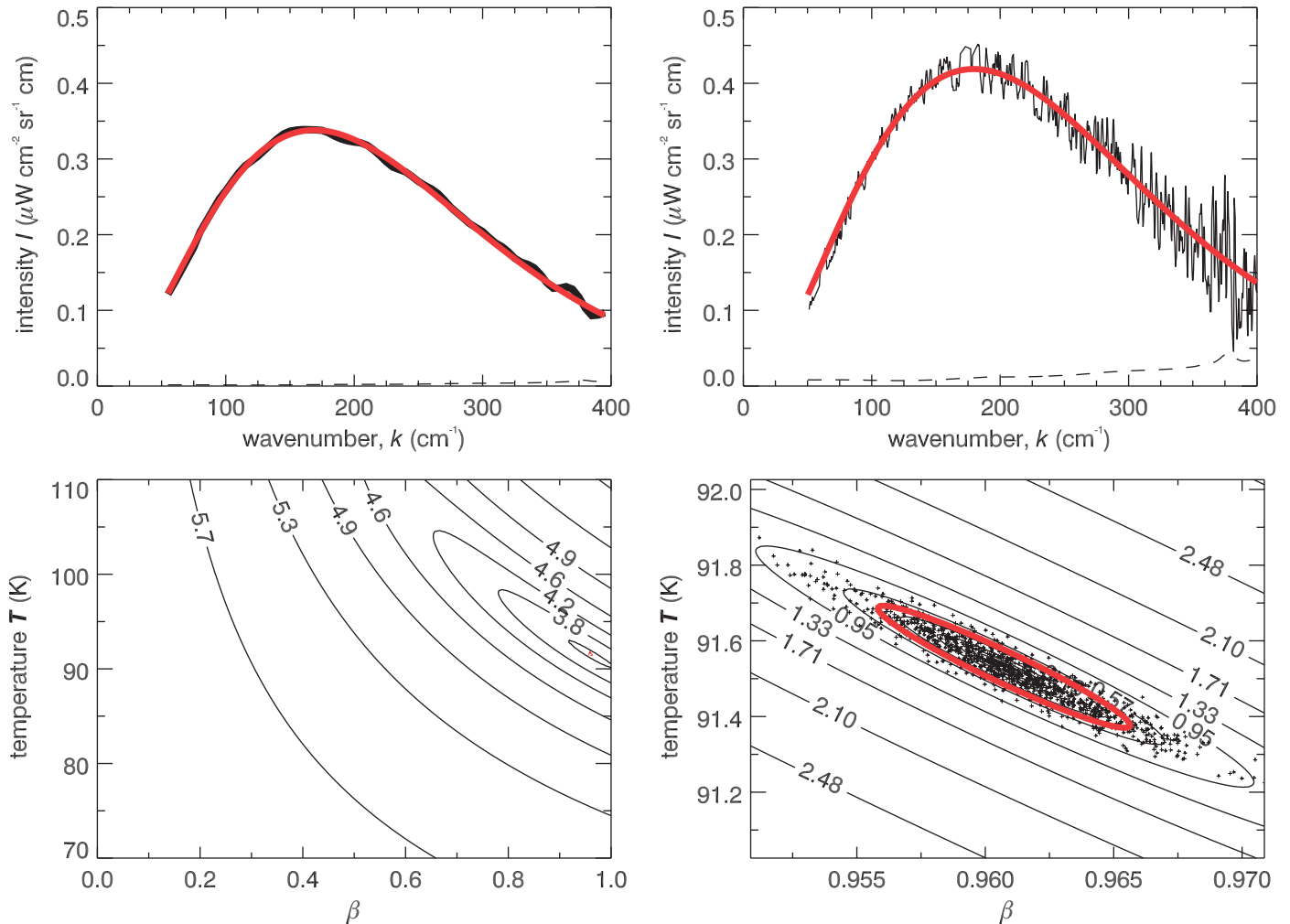


Fig. 2. The top two panels show examples of low and high spectral resolution spectra used in the fitting process. We show two spectra selected from the B ring at 105,000 km from Saturn. The top left panel is from the lit, high- α low-resolution (15.5 cm^{-1}) scan and the top right panel is from the lit, low- α high-resolution (1.0 cm^{-1}) scan (See Table 1 for details). Noise spikes have been removed from these spectra. Each spectrum is plotted with the best fit to the single-temperature Planck function. The NESR at these wave numbers are shown as dashed lines.

The bottom two panels show an example of the χ^2 fitting procedure for the high-resolution spectrum. The contours of $\log(\chi^2(T, \beta))$ are shown on the left over a large range of possible values. These contours are typical, and there are no local minima other than around the best fit (shown as a red dot). The right-hand panel is an expanded plot of the contours in the vicinity of the best fit. Here, the theoretical 1σ contour that we use in our error analysis is highlighted in red; the crosses represent the temperature and beta values derived from 1000 perturbations to the best fit spectrum, using uncorrelated, randomly generated noise with a standard deviation equal to the NESR at any wavenumber. In this realization 672 of the 1000 points lie within the theoretical contour, in close agreement with the expected 68%.

4.1. Temperature differences with phase angle

The four radial scans of the A, B and C rings and Cassini Division taken at different observing geometries are presented in Figs. 3 and 4. The CIRS temperature profiles are compared to the ring τ from the Voyager photopolarimeter (PPS) instrument (Esposito et al., 1983; Showalter et al., 2003), after smoothing to the effective CIRS FP1 radial resolution of $\sim 2300 \text{ km}$.

4.1.1. Lit rings

The temperatures on the lit face of the rings, at low and high phase, are shown in Fig. 3. The main rings are warmest on the lit face at low phase ($\alpha = 27\text{--}36^\circ$), with the

C ring and Cassini Division warmest of all, 95–105 K, while the B and A rings are cooler, 85–95 K. At high phase ($\alpha = 130\text{--}137^\circ$), the C ring is 8–15 K cooler and the A and B rings are 3–10 K cooler, indicating that the night hemispheres of the particles are cooler than their day hemispheres. The temperature difference ΔT with α indicates that at least the dominant radiators possess a significant temperature gradient across their surfaces.

The dominant trend across the ring system is a gross anti-correlation between τ and T at low α —the C ring and Cassini Division, which have $\tau < 0.3$, are observed to be considerably warmer than the A and B rings. They are also significantly warmer compared to the Voyager epoch, because the Sun is now much higher above the ring plane,

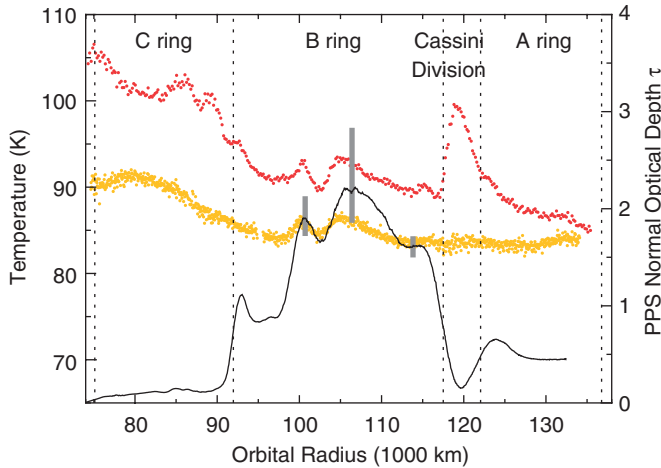


Fig. 3. Radial temperature variations across the lit rings at both low and high α . The ring temperatures at low α (red symbols) and high α (gold symbols) are shown as a function of ring radius, with the boundaries between rings indicated by dashed lines. Both scans were taken at afternoon local times. The C ring and Cassini Division exhibit the largest differences in temperature with α and are optically thinner than the A and B rings. The Voyager PPS τ profile is superposed, smoothed to the CIRS focal plane 1 (FP1) resolution. τ increases upward. The PPS τ that are plotted represent averages over the CIRS footprints. The central portion of the B ring is saturated in the PPS τ profile (no starlight penetrated the thickest parts of the B ring during the stellar occultation); so in order to take meaningful averages over the observation footprint, the saturated data points were replaced by averages of adjacent PPS data points. Vertical gray bars indicate the calibration uncertainty ($\pm 1\sigma$) in the PPS-derived optical depth in the B ring. Uncertainties in the less optically thick ring regions are narrower than the width of the line as plotted. Because this profile has been smoothed to ~ 2300 km, purely statistical uncertainties are negligible throughout. In the B ring, there is a good correlation between τ and temperature for both high and low α . Thermal contrast within the rings at high α is muted compared to the thermal contrast at low α .

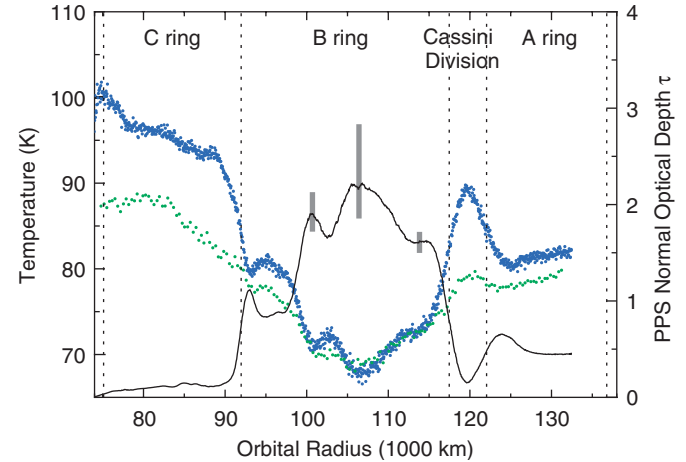


Fig. 4. Radial temperature variations across the unlit rings at both low and high α . The main ring temperatures at low α (blue symbols) and high α (green symbols) are shown as a function of ring radius. The radial resolution is 2000–2600 km. Both scans were taken at morning local times. The Voyager PPS τ profile is superposed, smoothed to the CIRS focal plane 1 (FP1) resolution. τ increases upward. Vertical gray bars indicate the calibration uncertainty ($\pm 1\sigma$) in the PPS-derived optical depth in the B ring. Uncertainties in the less optically thick ring regions are narrower than the width of the line as plotted. Because this profile has been smoothed to ~ 2300 km, purely statistical uncertainties are negligible throughout. The temperatures in the B ring are now anti-correlated with the τ .

decreases with increasing distance from Saturn. This suggests an increase in the number of smaller, and/or more rapidly rotating ring particles, which have more uniform surface temperatures. Perhaps this is caused stirring from the large number of density waves in the outer A ring and/or self-gravity wakes (Colwell et al., 2006).

Fig. 5a provides another perspective on these trends. Here, the temperature difference ΔT is plotted as a function of τ . Ring regions are color-coded: red for ring C, blue for ring B, green for ring A and yellow for the Cassini Division. Ignoring the A ring we see a relatively consistent trend with greater low-phase minus high-phase temperature changes in lower- τ rings. Albedo could be a contributing factor, because darker objects will heat up more efficiently in sunlight. The general correlation between optical depth and albedo has been noted from studies of the Voyager data (Doyle et al., 1989; Cooke, 1991; Dones et al., 1993). The A ring is quite exceptional on this plot, with much smaller temperature differences even though particle albedos are generally intermediate between rings B and C. The exceptional points are from the outermost region of the ring, which is the region with the greatest stirring by waves and wakes.

4.1.2. Unlit rings

Temperatures on the ring's unlit face (Fig. 4) show an almost perfect anti-correlation with τ . The C ring and Cassini division are still the warmest, almost certainly because their low optical depths allow even particles on the unlit face of the rings to be well illuminated by the Sun.

reducing the mutual shadowing between particles. The C ring and Cassini Division particles have lower visual albedos, lower optical depth τ , and reduced mutual shadowing, all of which contribute to their higher temperatures. This temperature difference was also observed by Voyager and interpreted as an albedo effect. In addition, in a vertically dispersed ring, the sunlit particles at the ring surface exchange heat with their cooler, subsurface neighbors, perhaps resulting in a higher effective thermal inertia in denser ring regions. At high α , the temperature variation with τ is similar but muted, consistent with the interpretation that one is seeing the unlit hemispheres of individual ring particles, where temperatures are closer to their equilibrium values.

However, within the optically thick A and B rings, the correlation between τ and T becomes distinctly positive, and stronger at low α . This appears at first to contradict the general conclusion above. At high enough τ , the sunlight does not penetrate so deeply into the ring so one explanation is that heat stays closer to the lit surface of the most optically thick rings. The lit A ring is particularly interesting because the magnitude of the thermal contrast

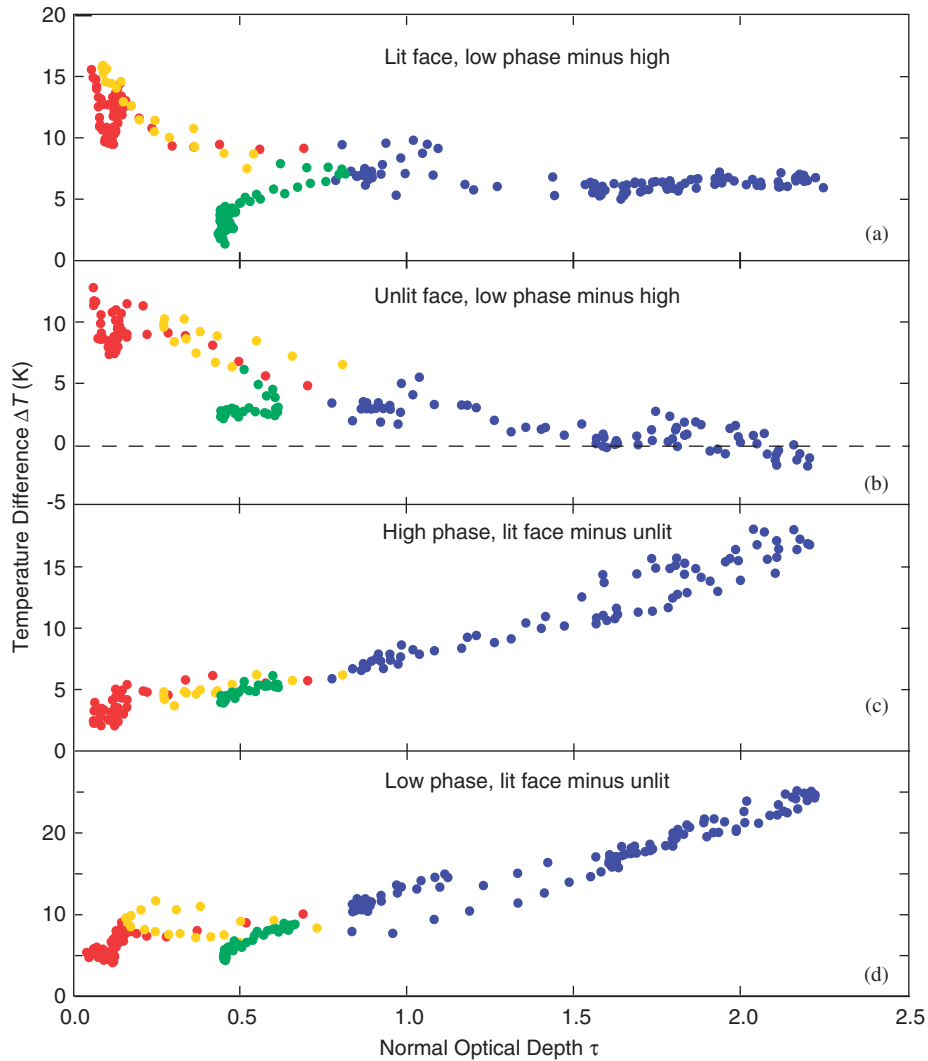


Fig. 5. Temperature variations within the rings are shown as a function of the PPS-derived optical depth τ . Individual rings are identified by color: A ring in green; B ring in blue; C ring in red; Cassini Division in yellow. (a) The hemispherical temperature variation of ring particles (low phase minus high) for the lit face of the rings. (b) Same as above but for the unlit face. (c) The temperature difference across the ring plane (lit face minus dark) at high-phase angles. (d) Same as above but for low phase. Strong trends are apparent in all four panels, although the A ring is anomalous in some regards, probably due to the strong stirring by density waves and wakes in its outer region.

The temperature variations with phase angle are similar to those seen for the lit rings (Fig. 3): the C ring and Cassini Division are again 10–15 K cooler at high α and the A ring is again a few K cooler. However, the optically thickest parts of the B ring are different. They have the same temperature at both high and low α , presumably because almost no sunlight reaches these particles, allowing them to reach thermal equilibrium across their surfaces.

Fig. 5b shows the data plotted as ΔT vs. τ . The general trend is almost identical to that on the lit side of the rings (Fig. 5a), except that temperature differences are smaller. We again suspect albedo as the primary cause of the trend, with stirring causing the outer part of ring A to be exceptional. Here ΔT goes to zero in the densest part of the B ring, presumably because sunlight has ceased to be a significant factor in the heating of these ring particles. Saturn still heats these particles, of course, but any

alternative heat sources will not show a dependence on solar phase angle.

4.2. Vertical temperature gradients

Fig. 5c and d shows the temperature difference vertically across the ring, lit face minus unlit face, for high and low phase, respectively. It should be noted that the lit measurements are from the afternoon ansa whereas the unlit measurements are from the morning ansa, so some variations may be related to orbital longitude rather than ring face. Nevertheless, the trends are clear and consistent among the different components of the rings: with higher τ , the temperature gradient across the ring increases. This makes intuitive sense: less sunlight reaches the dark face of the ring when τ is higher.

However, this may not provide the complete picture. For the optically thick B ring, almost no sunlight reaches the dark face regardless of the optical depth, so we might expect the value of ΔT to level off. Nevertheless, the trend from the less opaque rings into the B ring is continuous and almost linear. In part, this is because T and τ are positively correlated on the lit side of the B ring (Fig. 4a): not only is the dark face colder, but the lit face is warmer. For the B ring, this can be most easily understood if vertical mixing does not play a significant role. One way for heat to travel from the lit face to the dark face of a ring is by physical motion: for slightly inclined orbits, a particle on the lit face of the ring should have moved to the dark face 180° later, carrying its heat with it. Instead, it appears that high optical depth provides a significant obstacle to the vertical mixing of the ring particles. As noted above, simulations of high- τ rings do show a tendency toward multiple layers and reduced vertical mixing (Richardson, 1994). These CIRS results provide the first observational support for this phenomenon. However, more extensive dynamical and thermal modeling will be needed to understand this effect in more quantitative terms.

5. Discussion

To explain the temperature variation with α in Figs. 3 and 4, we require the presence of particles that can maintain a difference of at least 10–20 K between their lit and unlit sides. If they spin, they must have a low enough thermal inertia to gain and lose that much heat within a fraction of their spin period. As summarized above, the primary factors affecting the gradient in temperature from one side of a particle to the other are the size, spin rate, spin orientation (obliquity), thermal inertia, and the timescales on which the irradiating flux is changing. Particles that are small compared to the thermal wavelength for heat diffusion will reach thermal equilibrium fairly quickly, and would be expected to radiate fairly uniformly in all directions despite temporal variations in the irradiating field. To observe α effects, two requirements must be met. First, particles must be large enough for the thermal wave through the particle to propagate more slowly than the rotation period. Second, the thermal inertia must be low enough that surface temperature changes due to radiation are faster than the rotation period.

A point on a ring particle sees a variable flux that is related to its spin period. We expect particles illuminated by the Sun to experience a periodic flux due to day-night cycles and planetary shadow crossing at every orbit (annual cycle). The annual thermal skin depth $\delta_\Omega \sim \Gamma(2\Omega)^{1/2} \rho^{-1} C_p^{-1}$ is about 3.0–5.0 mm from C to A ring and the diurnal one $\delta_\omega \sim \Gamma(2/\omega)^{1/2} \rho^{-1} C_p^{-1}$ is of the order of 1.0–15 mm if the spin frequency ω ranges from 0.1–10 Ω , assuming typical values of $\Gamma = 15 \text{ J K}^{-1} \text{ m}^{-2} \text{ s}^{-1/2}$ and porosity = 0.5 (Ferrari and Leyrat, 2006). This range covers cases from retrograde spinning particles to particles spinning prograde many times per orbit. For comparison, the spin period will

range from 1 to 100 h for a typical orbital period of 10 h in the middle of the B ring. Particles that are small compared to δ will reach thermal equilibrium fairly quickly, and appear isothermal. When larger than about 3δ , particles will have different surface temperatures on their lit and unlit sides. As most particles in the rings are larger than a centimeter (French and Nicholson, 2000), thermal gradients between day and night sides are possible.

We construct a simple argument for the heat loss rate required for particles spinning with polar aligned axes. For this argument we ignore the heating by thermal radiation emitted by Saturn, sunlight reflected by Saturn, and sunlight reflected from other ring particles since these additional sources of heating represent 20% or less of the direct solar heating in the B ring (Aumann and Kieffer, 1973; Ferrari et al., 2005). Averaged over an orbital period the particles should be in thermal equilibrium and, on the average, they should be in rough equilibrium over their spin period, P , as well. If we consider a particle whose temperature fluctuates by some ΔT from lit to unlit side, then the amount of heat per unit area within the particle skin depth varies by approximately $\Delta Q \sim \rho C_p \Delta T \delta = 2\Gamma(P/\pi)^{1/2} \Delta T$. In the simplest case, we can consider the particle surface to pick up ΔQ (J m^{-2}) during the roughly half of its spin period when it is illuminated, and to get rid of that on the half of its rotation where it is unilluminated. This is in effect assuming we have a flat, two-sided particle which flips back and forth between being illuminated or not. In reality, each point on the particle surface is constantly heating or cooling, so our model assumes that, on the whole, the time average is that ΔQ (J m^{-2}) is picked up at any instant over the whole illuminated side, and hence the same must be being re-radiated on the unilluminated side. The characteristic time for radiating heat is then $t_{\text{char}} = \Delta Q / \sigma T_{\text{dark}}^4$ and in order to maintain a gradient, $t_{\text{char}} < P/2$, at most. So

$$P > (16/\pi) [\Gamma \Delta T / \sigma T_{\text{dark}}^4]^{2/3}. \quad (3)$$

Using a reasonable set of parameters for the B ring, let $\Gamma = 15$ ($\text{J K}^{-1} \text{ m}^{-2} \text{ s}^{-1/2}$), $\Delta T = 10$ K, and $T_{\text{dark}} = 85$ K, then $P > 3.6$ h. This estimate is the absolute minimum period allowable, since our observations are not at extremely low and extremely high α . Since we observe large temperature differences at moderate α , it is therefore prudent to conclude that t_{char} is actually much less than $P/2$. If we assume $P/5$, instead, it increases the minimum allowed spin period to 9 h for polar aligned spin axes. If in fact the axes have a distribution of orientations, then one will encounter cases where there is both faster and slower mechanical transport of heat from the lit to unlit side. To the accuracy of our crude calculations, we suggest that, if our observed thermal gradients are due to differences in particle temperatures from day to night side, there could be a population of particles whose spin periods are fairly close to synchronous.

6. Conclusions

Cassini CIRS observations of the A, B and C rings and Cassini Division provide spatially resolved thermal infrared scans that show ring particle temperatures decreasing with increasing α for both the lit and unlit faces of the rings. These temperature differences suggest that Saturn's main rings include a population of ring particles that are relatively large, spin slowly and have a low enough thermal inertia to provide a thermal response that is rapid compared to the particle rotation period.

The A ring has the smallest temperature variation with α , and this variation decreases even further with increasing ring radius. This decrease in thermal contrast suggests that A ring particles may rotate more rapidly, resulting perhaps from stirring by the larger number of density waves in the outer A ring and/or self-gravity wakes (Colwell et al., 2006).

The C ring and Cassini division are optically thin, have lower albedos, and show both warmer temperatures and larger temperature variations with α than do the optically thicker rings. As particle separation is increased, mutual obscuration and shadowing are reduced. Thus, for sparsely filled rings, e.g., the C ring, both the Sun and spacecraft have essentially unobstructed views of the lit and unlit faces (Froidevaux, 1981). This is consistent with the fact that the C ring and Cassini division have lower albedos than the A and B rings, as well as less mutual shadowing between ring particles.

In the B and A rings, to first order the temperature is correlated with τ on the lit face, and anti-correlated on the unlit face, consistent with the idea that little vertical mixing occurs in optically thick rings. In the B ring, the τ maxima correspond to the maximum B ring temperature on the lit face of the rings, while they correspond to the lowest temperatures on the unlit face of the rings. For the lit face, the persistence of the positive correlation with α could indicate that inter-particle heating is significant in the optically thick regions. It is expected that the optically thick regions would be the coldest in the unlit rings. The fact that the B ring temperature behaviors are reversed between the lit and unlit regions suggests that little sunlight is penetrating these regions, and that vertical mixing is not very efficient in the optically thickest parts of the rings.

7. Future observations

Observations at additional α , B , B' , and local times will be made throughout the remainder of the Cassini mission. These will enable us to more completely model ring particle thermal behavior and will provide additional constraints on particle rotation rates, spin direction and spin axis within each ring.

Acknowledgements

The authors gratefully acknowledge Paul Romani, Richard Achterberg and Conor Nixon for their help

designing and planning the CIRS ring observations. Thanks also to Thomas Spilker for helpful technical discussions and comments on the manuscript. We also acknowledge support from Judicael Decriem. This work was performed at the Jet Propulsion Laboratory, California Institute of Technology, under contract with the National Aeronautics and Space Administration.

References

- Araki, S., 1991. The dynamics of particle disks. III—Dense and spinning particle disks. *Icarus* 90, 139.
- Aumann, H., Kieffer, H., 1973. Determination of particle size in Saturn's rings from their eclipse cooling and heating curves. *Astrophys. J.* 186, 305–312.
- Colwell, J., Esposito, L., Sremčević, M., 2006. Self-gravity wakes in Saturn's A ring measured by stellar occultations from Cassini. *Geophys. Res. Lett.* 33, L07201.
- Cooke, M., 1991. Saturn's rings: photometric studies of the C Ring and radial variation in the Keeler Gap. Ph.D. Dissertation, Cornell University, xii + 206pp.
- Cuzzi, J., Lissauer, J., Esposito, L., Holberg, J., Marouf, E., Tyler, G., Boischot, A., 1984. Saturn's rings: properties and processes. In: Greenberg, R., Brahic, A. (Eds.), *Planetary Rings*. University of Arizona Press, pp. 73–199.
- Cuzzi, J., French, R., Dones, L., 2002. HST multicolour (255–1042 nm) photometry of Saturn's main rings. I. Radial profiles, phase and opening angle variations, and regional spectra. *Icarus* 158, 199–223.
- Dones, L., Cuzzi, J.N., Showalter, M.R., 1993. Voyager photometry of Saturn's A ring. *Icarus* 105, 184–215.
- Doyle, L.R., Dones, L., Cuzzi, J.N., 1989. Radiative transfer modeling of Saturn's outer B ring. *Icarus* 80, 104–135.
- Esposito, L., O'Callaghan, M., West, R., 1983. The structure of Saturn's rings: implications from the Voyager stellar occultation. *Icarus* 56, 439–452.
- Esposito, L., Cuzzi, J., Holberg, J., Marouf, E., Tyler, G., Porco, C., 1984. Saturn's rings: structure, dynamics, and particle properties. In: Gehrels, T., Matthews, M. (Eds.), *Saturn*. University of Arizona Press, pp. 463–545.
- Fernandez, Y., Jewit, D., Sheppard, S., 2002. Thermal properties of Centaurs Asbolus and Chiron. *Astrophys. J.* 123, 1050–1055.
- Ferrari, C., Leyrat, C., 2006. Thermal emission of spherical spinning ring particles: the standard model. *Astron. Astrophys.* 447, 745–760.
- Ferrari, C., Galdemard, P., Lagage, P.O., Pantin, E., Quoirin, C., 2005. Imaging Saturn's rings with CAMIRAS: thermal inertia of B and C rings. *Astron. Astrophys.* 441 (1), 379–389.
- Flasar, F., et al., 2004. Exploring the Saturn system with infrared eyes: the composite infrared spectrometer. *Space Sci. Rev.* 114 (1–4), 169–297.
- Flasar, F., et al., 2005. Temperatures, winds and composition in the Saturnian system. *Science* 307, 1247–1251.
- French, R., Nicholson, P., 2000. Saturn's Rings II. Particle sizes inferred from stellar occultation data. *Icarus* 145, 502–523.
- Froidevaux, L., 1981. Saturn's Rings: infrared brightness variation with solar elevation. *Icarus* 46, 4–17.
- Froidevaux, L., Ingersoll, A., 1980. Temperatures and optical depths of Saturn's rings and a brightness temperature for Titan. *J. Geophys. Res.* 85, 5929–5936.
- Froidevaux, L., Matthews, K., Neugebauer, G., 1981. Thermal response of Saturn's ring particles during and after eclipse. *Icarus* 46, 18–26.
- Groussin, O., Peschke, S., Lamy, P., 2000. Properties of 2060 Chiron from infrared ISOPHOT observations. *Bull. Am. Astron. Soc.* 32, 1031.
- Hanel, R., et al., 1981. Infrared observations of the Saturnian system from Voyager 1. *Science* 212, 192–200.
- Hanel, R., et al., 1982. Infrared observations of the Saturnian system from Voyager 2. *Science* 215, 544–548.

- Kunde, V., et al., 1996. Cassini infrared fourier spectroscopic investigation. *SPIE Proc.* 2803, 162–177.
- Ohtsuki, K., 2005. Rotation rates of particles in Saturn's rings. *Astrophys. J.* 626 (1), L61–L64.
- Ohtsuki, K., Toyama, D., 2005. Local N-body simulations for the rotation rates of particles in planetary rings. *Astron. J.* 130 (3), 1302–1310.
- Poulet, F., Cuzzi, J.N., French, R.G., Dones, L., 2002. The composition of Saturn's rings. *Icarus* 158, 224–248.
- Press, W., et al., 1992. *Numerical Recipes*. Cambridge Press Section 15.6, p. 690.
- Richardson, D.C., 1994. Tree code simulations of planetary rings. *Mon Not Roy Astron Soc* 269, 493.
- Roellig, T., Werner, M., Becklin, E., 1988. Thermal emission from Saturn's rings at 380 microns. *Icarus* 73, 574–583.
- Salo, H., 1987. Numerical simulations of collisions between rotating particles. *Icarus* 70, 37–51.
- Salo, H., 1995. Simulations of dense planetary rings. *Icarus* 117, 287–312.
- Salo, H., Karjalainen, R., 2003. Photometric modeling of Saturn's rings I. Monte Carlo method and the effect of nonzero volume filling factor. *Icarus* 164 (2), 428–460.
- Schulman, L., 2004. The heat capacity of water ice in interstellar or interplanetary conditions. *Astron. Astrophys.* 416, 187–190.
- Showalter, M. R., et al., 2003. USA_NASA_PDS_VG_2801, NASA Planetary Data System.
- Slack, G., 1980. Thermal conductivity of ice. *Phys. Rev. B* 22, 3065–3071.
- Smith, et al., 1981. Encounter with Saturn, Voyager 1 imaging results. *Science* 212, 163–191.
- Spencer, J., Moore, J., 1992. The influence of thermal inertia on temperatures and frost stability on Triton. *Icarus* 99, 261–272.
- Spencer, J., Lebofsky, L., Sykes, M.V., 1989. Systematic biases in radiometric diameter determinations. *Icarus* 78, 337–354.
- Spencer, J., Pearl, J., Segura, M., Flasar, F.M., Mamoukine, A., Romani, P., Buratti, B., Hendrix, A., Spilker, L., Lopes, R., 2006. Cassini encounters Enceladus: background and the discovery of a south polar hot spot. *Science* 311, 1401–1405.
- Spilker, L., Ferrari, C., Cuzzi, J., Showalter, S., Pearl, J., Wallis, B., 2003. Saturn's rings in the thermal infrared. *Planet. Space Sci.* 51, 929–935.
- Spilker, L., et al., 2005. Cassini CIRS: thermal changes in Saturn's main rings with increasing phase angle. *Bull. Am. Astron. Soc.* 37 (3), 764.
- Spilker, L., Pilorz, S., Wallis, B., Edgington, S., Brooks, S., Pearl, J., Flasar, F., 2006. Cassini CIRS Observations of a roll-off in Saturn ring spectra at submillimeter wavelengths. *Earth, Moon and Planets* 96, 149–163.